International Journal of Notural and Engineering Sciences
Uluslararası Doğa ve Mühendislik Bilimleri Dergisi
E-ISSN: 2146-0086, 11 (2): 23-30, 2017, www.nobel.gen.tr

Design of an Electromechanical Fin Actuation Mechanism and Experimental Study of Power Consumption of the Mechanism

Murat YILMAZ[1*] Ahmet Özdemir[2]
[1]Department of Manufacturing Engineering, Gazi University, Ankara, TURKEY
[2]Department of Manufacturing Engineering, Gazi University, Ankara, TURKEY

*Corresponding Author
E-mail: muratyilmaz89@hotmail.com

Received: May 20, 2017
Accepted: August 10, 2017

Abstract

Fixed-wing flying objects use control surface (fin) motions to balance and adjust flight directions. Mechanisms used to move control surfaces can be designed as hydraulic, pneumatic or electromechanical. In this study, an electromechanical fin actuation mechanism is designed. The kinematic equations of this the mechanism are derived and position, velocity and acceleration analyses are performed. The results obtained from these analyses are used as an input in the dynamic equations which include friction to calculate the power consumption of the mechanism. A test bench is used to investigate the accuracy of the analytical model. The mechanism is tested on the test bench under certain fin loads and speeds. The power consumption of the mechanism is found and compared with the results which are obtained from the analytical model. Tests are repeated for different fin loads, speeds and the cases (ball bearing or bushing) to verify the results of the analytical model. The results obtained from the tests and analytical model show that, the difference between them does not exceed 8%. Due to uncertainties of the measurement technique and uncertainties of friction coefficients, it is can be said that the results obtained from the tests are acceptable for the verification of the analytical model.

Keywords: Analytic motion analysis, Computer aided motion analysis, Experimental kinematic and dynamic analysis, Power consumption, Fin actuation mechanism

INTRODUCTION

Fixed-wing flying objects use control surface (fin) motions as shown in Figure 1 to balance and adjust flight directions.

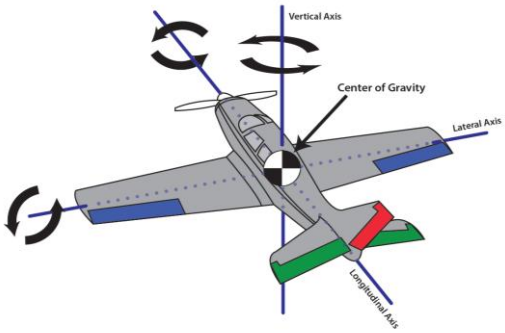

Figure 1. Fixed-wing flying objects motions.

Fin movements are required for fixed-wing flying objects to perform these maneuver motions. To provide these motions, fin actuation mechanisms are required.

Fin actuation mechanisms can be designed as hydraulic, pneumatic or electromechanical [1]. However, recent trend in aerospace industry is "More Electric Design". For this reason, nowadays fin actuation mechanisms are designed as electromechanical systems [2].

A great deal of research effort has been directed to design the electromechanical fin actuation system for fixed wing air vehicles [3], [4], [5] and [6]. Common points in these designs are the components which are used in mechanisms. These components are electric motor, planetary gearbox and ball screw. Electric motors are used to drive the mechanism, planetary gearboxes are used to achieve the desired transmission ratio and ball screws are used to convert the circular motion of the electric motors into a linear motion.

The performance of the mechanisms needs to be tested so that the fin actuation mechanisms can be used in fixed wind air vehicles [7]. For this reason the test benches are designed to measure the performance of the mechanisms against the aerodynamic forces [8]. These test benches have a torque motor to simulate aerodynamic forces and a position sensor to measure the fin position.

SYSTEM DESCRIPTION

Position, Velocity and Acceleration Analysis of Fin Actuation Mechanism

For this study, inverted slider crank mechanisms are investigated as a fin actuation mechanism. Figure 2 shows the schematic representation of the mechanism.

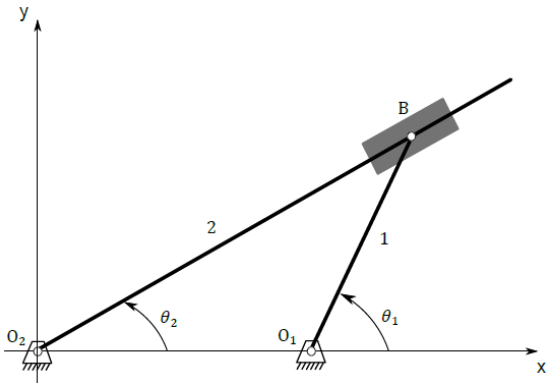

Figure 2. Schematic representation of the mechanism

Link 2 and B prismatic joint of the mechanism represent the electric motor and nut of the ball screw, respectively. Link 1 and O_1 represent leverage arm which is connect to the fin and hinge of the fin, respectively.

The vector representation of the mechanism is shown in Figure 3.

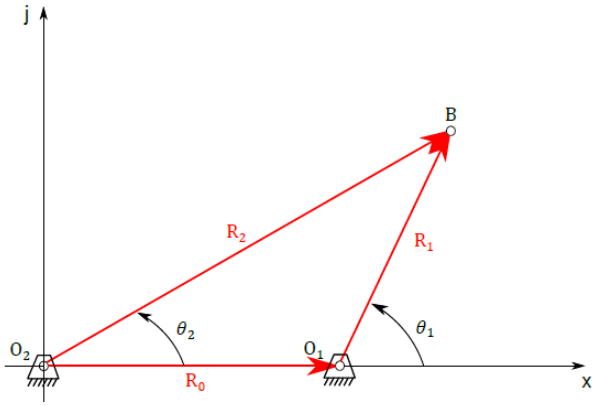

Figure 3. Vector representation of the mechanism

Loop closure equation must be written in order to analyze the position of the links in the mechanism. Loop closure equation of the mechanism according to Figure 3 can be given as;

$$R_2 e^{j\theta_2} = R_0 + R_1 e^{j\theta_1} \quad (1)$$

Eq. (1) can be expanded as shown in Eq. (2).

$$R_2 \cos\theta_2 + jR_2 \sin\theta_2 = R_0 + R_1 \cos\theta_1 + jR_1 \sin\theta_1 \quad (2)$$

Solving Eq. (2) gives the positions of the links in the mechanism.

Velocity parameters of the mechanism are shown in Figure 4.

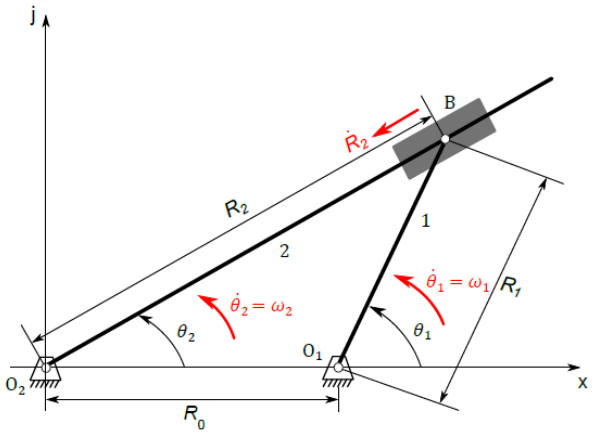

Figure 4. Velocity parameters of the mechanism

By differentiating the Eq. (1), velocities of the links in the mechanism can be found as in Eq. (3).

$$j\frac{d\theta_2}{dt}R_2 e^{j\theta_2} + \frac{dR_2}{dt}e^{j\theta_2} = j\frac{d\theta_1}{dt}R_1 e^{j\theta_1} \quad (3)$$

Where,

$$\frac{d\theta}{dt} = w$$

and

$$\frac{dR_2}{dt} = v_B$$

Then the equation becomes,

$$j\omega_2 R_2 e^{j\theta_2} + v_B e^{j\theta_2} = j\omega_1 R_1 e^{j\theta_1} \quad (4)$$

When both sides of the equation is multiplied by $e^{-j\theta_2}$,Eq. (5) is obtained,

$$j\omega_2 R_2 + v_B = j\omega_1 R_1 e^{j(\theta_1 - \theta_2)} \quad (5)$$

Eq. (5) can be expanded as shown in Eq. (6).

$$j\omega_2 R_2 + v_B = j\omega_1 R_1 \cos(\theta_1 - \theta_2) - \omega_1 R_1 \sin(\theta_1 - \theta_2) \quad (6)$$

Solving Eq. (6) gives the velocities of the links in the mechanism.

Acceleration parameters of the mechanism are shown in Figure 5.

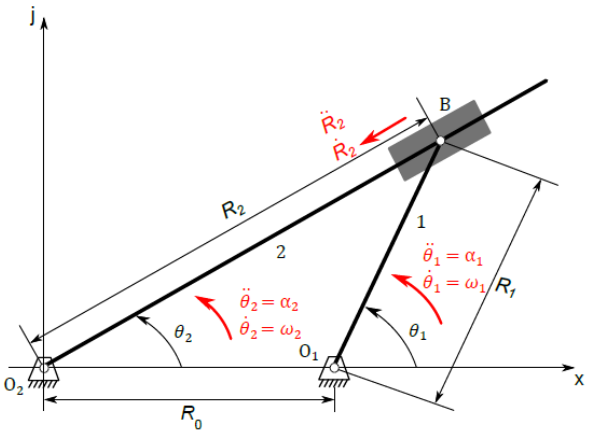

Figure 5. Acceleration parameters of the mechanism

By differentiating the Eq. (3), accelerations of the links in the mechanism can be found as in Eq. (7).

$$-\omega_2^2 R_2 e^{j\theta_2} + j\frac{d\omega_2}{dt} R_2 e^{j\theta_2} + j\omega_2 \frac{dR_2}{dt} e^{j\theta_2} + j\omega_2 v_B e^{j\theta_2} + \frac{dv_B}{dt} e^{j\theta_2} = -\omega_1^2 R_1 e^{j\theta_1} + j\frac{d\omega_1}{dt} R_1 e^{j\theta_1} \quad (7)$$

Where,

$$\frac{d\omega}{dt} = \alpha$$

and

$$\frac{dv_B}{dt} = a_{B_1B_2}^t$$

Then the equation becomes,

$$-\omega_2^2 R_2 e^{j\theta_2} + j\alpha_2 R_2 e^{j\theta_2} + 2j\omega_2 v_B e^{j\theta_2} + a_{B_1B_2}^t e^{j\theta_2} = -\omega_1^2 R_1 e^{j\theta_1} + j\alpha_1 R_1 e^{j\theta_1} \quad (8)$$

When both sides of the equation is multiplied by $e^{-j\theta_2}$, Eq. (9) is obtained,

$$-\omega_2^2 R_2 + j\alpha_2 R_2 + 2j\omega_2 v_B + a_{B_1B_2}^t = (-\omega_1^2 + j\alpha_1) R_1 e^{j(\theta_1 - \theta_2)} \quad (9)$$

Eq. (9) can be expanded as shown in Eq. (10).

$$-\omega_2^2 R_2 + j\alpha_2 R_2 + 2j\omega_2 v_B + a_{B_1B_2}^t = [-\omega_1^2 \cos(\theta_1 - \theta_2) - \alpha_1 \sin(\theta_1 - \theta_2) - j\omega_1^2 \sin(\theta_1 - \theta_2) + j\alpha_1 \cos(\theta_1 - \theta_2)]R_1 \quad (10)$$

Dynamic Force Analysis of Fin Actuation Mechanism

Using the equations (1) – (10) position, velocity and acceleration of the links of the mechanism can be found. Then the force analysis can be performed. Force and moment equations should be written by using the free body diagram of the links.

The free body diagram of the first link is given in the following Figure.

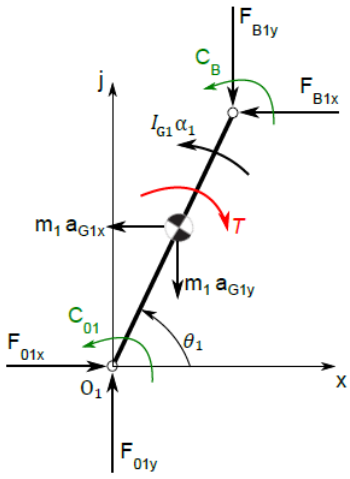

Figure 6. Free body diagram of first link.

Where C_{01} and C_B shows the frictional torque that occurs in joints due to friction of the ball bearings/bushings. T is the aerodynamic force which is applied to the fin.

Force and moments equations can be obtained as in Eq. (11) –Eq. (13) using the free body diagram of the first link;

$$\sum F_x = F_{O1_x} - F_{B1_x} = m_1 a_{G1_x} \quad (11)$$

$$\sum F_y = F_{O1_y} - F_{B1_y} = m_1 a_{G1_y} \quad (12)$$

$$\sum M_{G1} = F_{B1_x}\frac{R_1}{2}\sin\theta_1 - F_{B1_y}\frac{R_1}{2}\cos\theta_1 + F_{O1_x}\frac{R_1}{2}\sin\theta_1 - F_{O1_y}\frac{R_1}{2}\cos\theta_1 - T + \mu_{O1} r_{O1}\left({F_{O1_x}}^2 + {F_{O1_y}}^2\right)^{\frac{1}{2}} sign(\omega_0 - \omega_1) + \mu_{B1} r_{B1}\left({F_{B1_x}}^2 + {F_{B1_y}}^2\right)^{\frac{1}{2}} sign(\omega_B - \omega_1) = I_{G1}\alpha_1 \quad (13)$$

Where μ and r are friction coefficient and radius of the ball bearing/bushing, respectively.

The free body diagram of the prismatic joint is given in the following Figure.

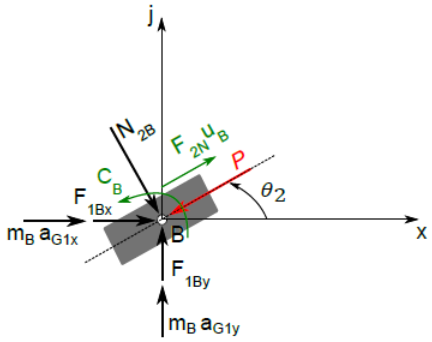

Figure 7. Free body diagram of prismatic joint.

Where C_B shows frictional torque that occurs in joint due to the friction of the ball bearings/bushings and $F_{2N}\mu_B$ shows the frictional force in ball screw. P is the force acting on the ball screw.

Force and moments equations can be obtained as in Eq. (14) – Eq. (16) using the free body diagram of the prismatic joint;

$$\sum F_x = F_{1B_x} - P\cos\theta_2 + N_{2B}\sin\theta_2 + \mu_{B2}|N_{2B}\cos\theta_2|\, sign(v_{B_1B_2}) = m_B a_{B_x} \quad (14)$$

$$\sum F_y = F_{1B_y} - P\sin\theta_2 - N_{2B}\cos\theta_2 + \mu_{B2}|N_{2B}\sin\theta_2|\, sign(v_{B_1B_2}) = m_B a_{B_y} \quad (15)$$

$$\sum M_{GB} = \mu_{B2} h |N_{2B}|\, sign(v_{B_1B_2}) + \mu_{B1} r_{B1} \left({F_{1B_x}}^2 + {F_{1B_y}}^2\right)^{\frac{1}{2}} sign(\omega_B - \omega_1) = 0 \quad (16)$$

The free body diagram of the second link is given in the following Figure.

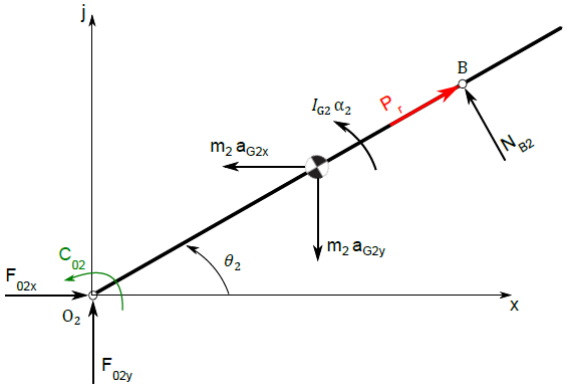

Figure 8. Free body diagram of second link.

Where C_{02} frictional torque that occurs in joints due to friction of the ball bearings/bushings.

Force and moments equations can be obtained as in Eq. (17) – Eq. (19) using the free body diagram of the second link;

$$\sum F_x = F_{O2_x} + P_r\cos\theta_2 - N_{B2}\sin\theta_2 = m_2 a_{G2_x} \quad (17)$$

$$\sum F_y = F_{O2_y} + P_r\sin\theta_2 + N_{B2}\cos\theta_2 = m_2 a_{G2_y} \quad (18)$$

$$\sum M_{G2} = F_{O2_x}\frac{R_2}{2}\sin\theta_2 - F_{O2_y}\frac{R_2}{2}\cos\theta_2 + N_{B2}\frac{R_2}{2} - P_r\cos\theta_2\frac{R_2}{2}\sin\theta_2 + P_r\sin\theta_2\frac{R_2}{2}\cos\theta_2 + \mu_{O2} r_{O2}\left({F_{O2_x}}^2 + {F_{O2_y}}^2\right)^{\frac{1}{2}} sign(\omega_0 - \omega_2) = I_{G2}\alpha_2 \quad (19)$$

P that is produced by electric motor and acting on the ball screw is found by solving Eq. (11) – Eq. (19) numerically.

Calculation of Power Consumption of Electric Motor

To calculate the power, consumed by an electric motor, torque and angular speed of the electric motor must be known.

Torque that should be produced by electric motor to create the P force that is obtained from the dynamic force analysis, can be calculated as following,

$$T_m = \frac{T_{sh} + T_i}{N_d\,\mu_d} \quad (20)$$

In Eq. (20), T_m is the torque that should be produced by electric motor, T_{sh} is the torque that should be produced by the electric motor with constant velocity assumption and T_i is the torque that should be produced by the electric motor considering also the effects of acceleration.

N_d and μ_d shows the transmission ratio of the gearbox and gearbox efficiency, respectively.

$$T_{sh} = T_y + T_o + T_s \quad (21)$$

In Eq. (21), T_y is the torque that the mechanism should produce against the aerodynamic force, T_o is the torque that is occurred due to the preload force applied to decrease the gap in ball screw and finally T_s is the friction force occurs in the bearings used for mounting the ball screw to gearbox.

$$T_y = \frac{P\,.H}{2000\pi\mu_{bv}} \quad (22)$$

In eq (22), P is the force that should be applied by ball screw against the aerodynamic force and it is calculated by the equations given in dynamic force analysis section; H is the pitch of the ball and μ_{bv} is the efficiency of ball screw.

$$T_i = I_t\alpha_m \quad (23)$$

In Eq. (23), I_t is the total inertia of the electric motor and ball screw and α_m is the angular acceleration of the motor.

Prototype and Test Bench

The fin actuation mechanism model used in this study is shown in Figure 9.

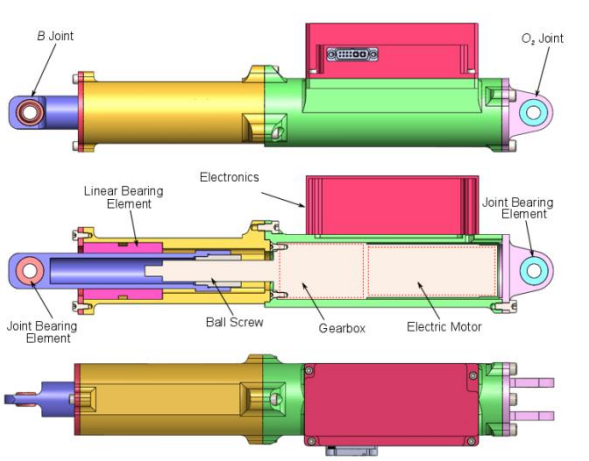

Figure 9. Model of the fin actuation mechanism.

Electric motor is mounted to the body part shown in green. Piston that is shown in purple is mounted to the ball screw that is integrated with electric motor. This piston moves the fin by linear motion of the ball screw that is mounted to linear bearing shown in pink. Piston that is shown in purple simulates the prismatic joint which is shown in Figure 1. The joint located at the end of the piston simulates the B joint which is shown in Figure 2.

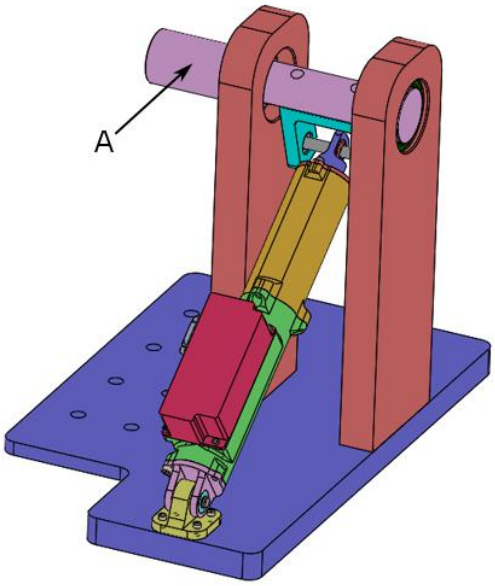

Figure 10. Fin actuation mechanism model mounted on the test bench fixture.

The shaft shown as "A" in Figure 10 is the fin shaft of the mechanism. This shaft is fastened to the test bench shaft by coupling and it transmits the aerodynamic loads produced by load motor in the test bench.
The prototype of the fin actuation mechanism and the test bench fixture is given in Figure 11.

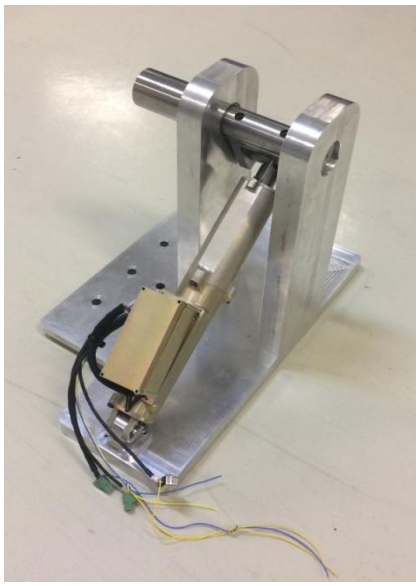

Figure 11. Fin actuating mechanism mounted on the test bench fixture.

Tests

The position and load commands given as an example in Figure 12 is applied to the mechanism in the tests. The power consumed by the electric motor during the tests is measured. The results obtained from the tests are compared with the results of the analytical model.

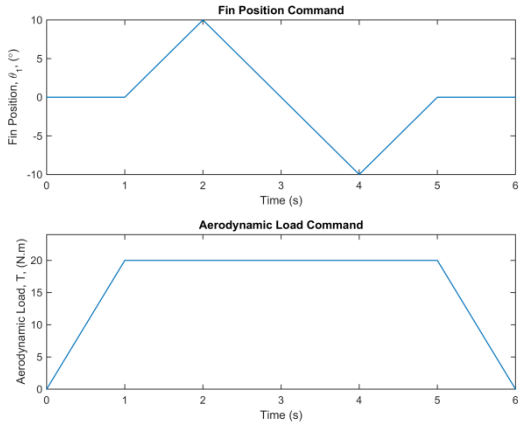

Figure 12. Position and load command.

Three parameters have been changed during the tests. These parameters and their values are given below;

- Angular velocity of first link (ω_1); It is changed from 10°/s to 100°/s with 10°/s intervals,
- Aerodynamic load on the first link (T); It is changed from 10 N.m to 40 N.m with 10 N.m intervals,
- Bearings which is used in joints; all the bearings in the fin actuation mechanism have been tested in two different configurations as ball bearing and bushing,

Parameters that are taken into account when calculating the analytical model results are given in Table 1 and Table 2 for the mechanism and for the electric motor and power train, respectively.

Table 1. Parameters of Mechanism

Parameter	Symbol	Value
Length of the fixed link	R0	299,84 mm
Length of the first link	R1	50 mm
Mass of the first link	m1	0,147 Kg
Mass of the second link	m2	0,819 Kg
Mass of the prismatic joint	mb	0,127 Kg
Inertia of the first link	I_1	17,2 e^{-6} Kg.mm^2
Inertia of the second link	I_2	6893,7 e^{-6} Kg.mm^2
Friction coefficient of ball bearings [9]	μ_{O1}, μ_{O2}, μ_{B1} and μ_{B2}	0,0015
Radius of the ball bearings in O_2 and B joints	r_{O2} and r_{B1}	8 mm
Radius of the ball bearings in O_1 joint	r_{O1}	20 mm
Friction coefficient of bushings [10]	μ_{O1}, μ_{O2}, μ_{B1} and μ_{B2}	0,2
Radius of the bushings in O_2 and B joints	r_{O2} and r_{B1}	9 mm
Radius of the bushings in O_1 joint	r_{O1}	16 mm

Table 2. Parameters of Electric Motor and Power Train

Parameter	Symbol	Value
Transmission ratio of gearbox	N_d	3,7
Efficiency of gearbox	μ_d	0,8
Efficiency of ball screw	μ_{bv}	0,9
Pitch of ball screw	H	2 mm
Inertia of electric motor	I_m	33,3e^{-7} Kg.m^2
Inertia of ball screw	I_{bv}	21,7e^{-7} Kg.m^2
Preload torque of ball screw	T_O	0,01 N.m
Friction torque of gearbox	T_s	0,01 N.m

RESULTS AND DISCUSSION

Test Results

The differences between the results obtained from the tests and the results of the analytical model are given in Figure 13 – Figure 20.

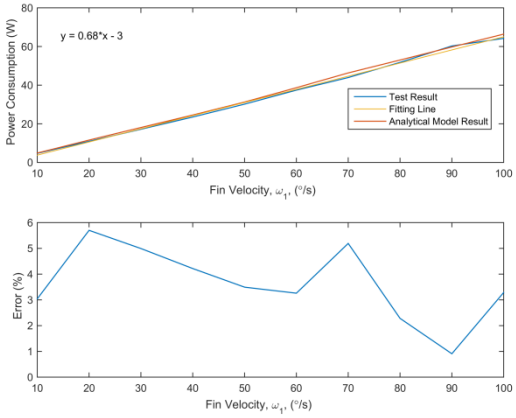

Figure 13. Power consumption under 10 N.m aerodynamic load.

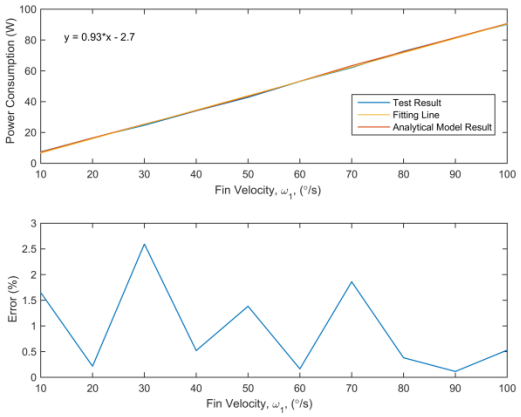

Figure 14. Power consumption under 20 N.m aerodynamic load.

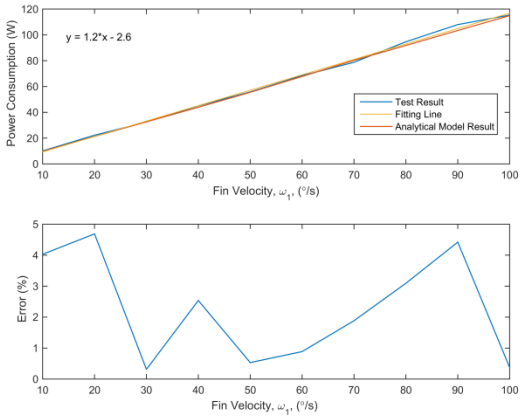

Figure 15. Power consumption under 30 N.m aerodynamic load.

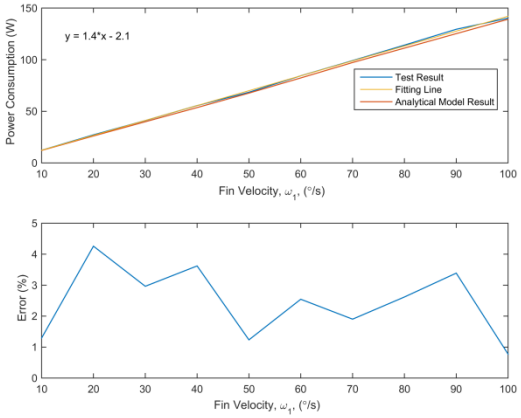

Figure 16. Power consumption under 40 N.m aerodynamic load.

Power consumption of the mechanism that has ball bearings in its joints are given in Figure 13 - Figure 16. As seen in the Figures, the results of the test and analytical model are consistent with each other. The error between the results does not exceed 6%. Due to the uncertainties of the measurement technique and the uncertainties of friction coefficients, it can be said that the results obtained from the tests are acceptable for the verification of the analytical model.

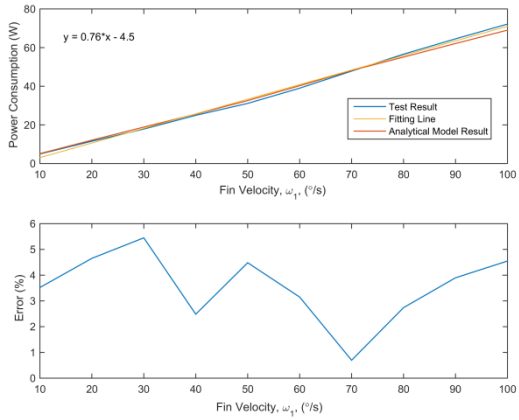

Figure 17. Power consumption under 10 N.m aerodynamic load.

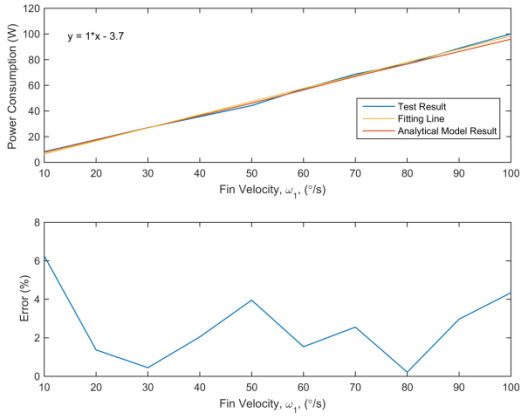

Figure 18. Power consumption under 20 N.m aerodynamic load.

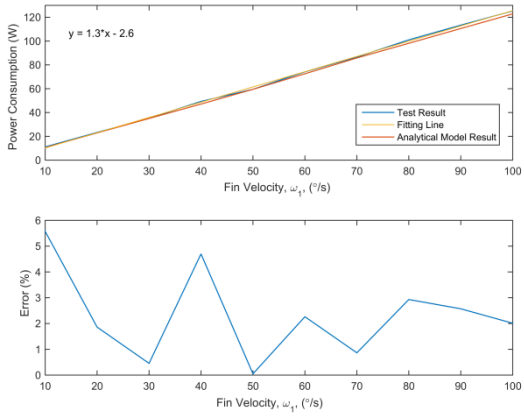

Figure 19. Power consumption under 30 N.m aerodynamic load.

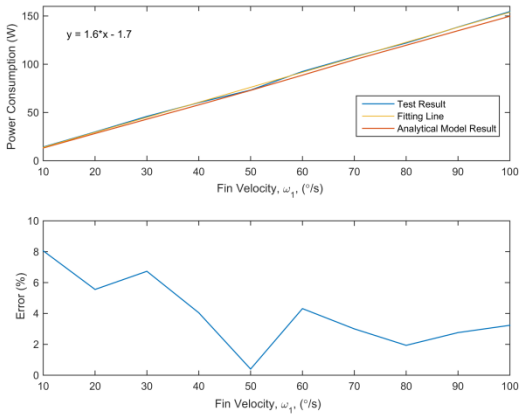

Figure 20. Power consumption under 40 N.m aerodynamic load.

Power consumption of the mechanism that has bushings in its joints is given in Figure 17 - Figure 20. As seen in the Figures, the test results and the analytical model results are consistent with each other. The error between the results does not exceed 8%. Due to uncertainties of the measurement technique and the uncertainties of friction coefficients, it can be said that the results obtained from the tests are acceptable for the verification of the analytical model.

As seen in the test results, the power consumption of the electric motor increases as the aerodynamic load and the angular velocity of the fin increase. Increase in power consumption due to the aerodynamic load and the angular velocity of the fin is expected due to the equation given in Eq. (24).

$$Power = Torque\ .\ Angular\ Velocity \tag{24}$$

Power consumption of the mechanism that has bushings in its joints is higher than the mechanism that has ball bearings in its joints. The reason for that are the friction forces. The frictional forces are more prominent in the mechanism that has bushings in its joints because the friction coefficient of the bushings is higher than that of the ball bearing.

The difference in power consumption between the mechanism that has bushings and ball bearings in its joints is given in Figure 21.

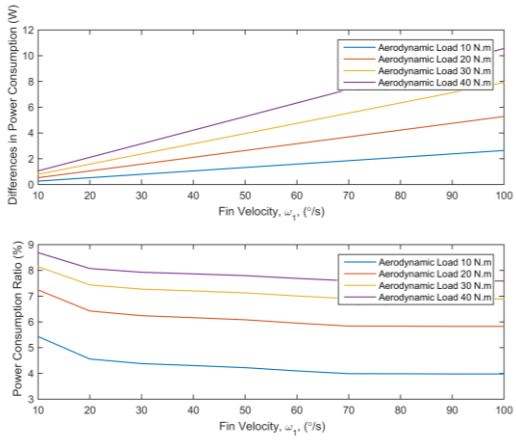

Figure 21. Power consumption differences of the mechanism that has bushings/ball bearing in its joints.

Figure 21 shows that the difference in power consumption between the two mechanism increases as the aerodynamic forces increase because the friction coefficient of the bushing is too high compared to the ball bearing. If the difference in power consumption is proportional to the amount of power consumed, it is seen that the fin velocity dependent changes in power consumption is quite low. As the power consumption ratio is higher at lower fin velocities, it is considered that friction at the lower velocities in bearing elements acts like a static friction.

CONCLUSION

This paper provides analytical and experimental test results about the effect of the bearing elements on the power consumption of inverted slider crank mechanism used as a fin actuation mechanism.

There are power restrictions in fixed-wing flying objects that provide electrical power from batteries like an unmanned aerial vehicle and missile. Engineers need to consider these power constraints when choosing the bearing elements used in the fin actuation mechanisms and test it to determine the power consumption of the mechanism. However, this paper has shown that the analytical model can be used to calculate the power consumption of the mechanism, accurately. The main advantage of that is the power consumption of the fin actuation mechanism can be found by analytical model, eliminating the test bench, time consumption and human resource required for testing.

REFERENCES

[1] Fleeman, E. L. (2006). *Tactical Missile Design.* (Second edition). Virginia: American Institute of Aeronautics and Astronautics, pp. 36 – 48.

[2] Wheeler, P. The More Electric Aircraft - Why Aerospace Needs Power Electronic. URL:http://www.webcitation.org/query?url=http%3A%2F%2Fwww.lboro.ac.uk%2Fmicrosites%2Fresearch%2Fiemrc%2FEvents%2520write%2520up%2FPower%2520Electronics%252014.05.09%2FMore_Electric_Aircraft_000.pdf&date=2017-11-13, Date of Access: 13.11.2017.

[3] Whitham, K. (2004). *Apparatus and method for fin actuation in a portable missile*. United States Patent, pp. 1 – 8.

[4] Wingett, P., Gaines, L. T., Evans, P. S. and Kern, I. (2006). *Flight control actuation system.* United States Patent, pp. 1 – 8.

[5] Hastürk, Ö. (2015, July). *A novel electromechanical actuator for missile jet vane thrust control.* International Conference on Advanced Intelligent Mechatronics, Busan, Korea.

[6] Jensen, S. C., Jenney, G. D. and Dawson, D. (2000, October). *Flight test experience with an electromechenical actuator on the F-18 System Research Aircraft*. Paper presented at the Digital Avionics Systems Conference, Philadelphia, USA.

[7] Antonelli, M. G., Bucci, G., Ciancetta, F. And Fiorucci, E. (2014, August). Automatic test equipment for avionics electro-mechanical actuators (EMAs). *Measurement*, pp. 71 – 84.

[8] Ristanovic, M., Cojbasic, Z. and Lazic, D. (2012, March). Intelligent control of DC motor driven electromechanical fin actuator. *Control Engineering Practice*, pp. 610 – 617.

[9] SKF. Estimating the Frictional Moment. URL:http://www.webcitation.org/query?url=http%3A%2F%2Fwww.skf.com%2Fgroup%2Fproducts%2Fbearings-units-housings%2Fball-bearings%2Fprinciples%2Ffriction%2Festimating-frictional-moment%2Findex.html&date=2017-11-13, Date of Access: 13.11.2017.

[10] SKF. (2017). *SKF Bushings, Thrust Washers and Strips.* Göteborg, Swedish, pp. 18 – 20.